Journal of Zhejiang University-SCIENCE C (Computers & Electronics)
ISSN 1869-1951 (Print); ISSN 1869-196X (Online)
www.zju.edu.cn/jzus; www.springerlink.com
E-mail: jzus@zju.edu.cn

Human-machine interaction force control: using a model-referenced adaptive impedance device to control an index finger exoskeleton*

Qian BI, Can-jun YANG‡

(*State Key Laboratory of Fluid Power Transmission and Control, Zhejiang University, Hangzhou 310027, China*)

E-mail: biqianmyself@zju.edu.cn; ycj@zju.edu.cn

Received Sept. 16, 2013; Revision accepted Dec. 29, 2013; Crosschecked Mar. 17, 2014

Abstract: Exoskeleton robots and their control methods have been extensively developed to aid post-stroke rehabilitation. Most of the existing methods using linear controllers are designed for position control and are not suitable for human-machine interaction (HMI) force control, as the interaction system between the human body and exoskeleton is uncertain and nonlinear. We present an approach for HMI force control via model reference adaptive impedance control (MRAIC) to solve this problem in case of index finger exoskeleton control. First, a dynamic HMI model, which is based on a position control inner loop, is formulated. Second, the theoretical MRAC framework is implemented in the control system. Then, the adaptive controllers are designed according to the Lyapunov stability theory. To verify the performance of the proposed method, we compare it with a proportional-integral-derivative (PID) method in the time domain with real experiments and in the frequency domain with simulations. The results illustrate the effectiveness and robustness of the proposed method in solving the nonlinear HMI force control problem in hand exoskeleton.

Key words: Interaction force, Adaptive control, Exoskeleton, Human-machine interaction (HMI), Impedance
doi:10.1631/jzus.C1300259 **Document code:** A **CLC number:** TP242.3

1 Introduction

Exoskeleton robots have been developed to replace traditional therapist-dependent post-stroke rehabilitation. Current robotic systems can assist movement in a number of different modes (Prange *et al*., 2006), including passive assist mode, in which the patients relax while the exoskeleton performs limb movements, and active assist mode, in which the patients attempt to move and the exoskeleton supplements the effort (Takahashi *et al*., 2008). In particular, passive assist mode emphasizes that the exoskeleton could drive the limb to follow the desired position in the range of motion (ROM). Usually, the input reference signal of the control system is a position variable. In active assist mode, however, the control target is an interaction force. Since the force reflects the motion attempts, we can provide the effort for the movement by controlling the interaction force between the human and exoskeleton (Huo *et al*., 2011).

However, human hand is the most dexterous part of the human body, including five fingers and 22 degrees of freedom (DOFs). Development of hand exoskeletons has proceeded slowly in terms of both the mechanism and the control method. Most of the hand exoskeleton control methods focus on passive assist mode, i.e., position control. The simplest method is using a commercial motor driver to achieve the precise position control of a motor. Ueki *et al*. (2012) presented a novel virtual reality (VR) enhanced hand rehabilitation support system con-

‡ Corresponding author

* Project supported by the National Natural Science Foundation of China (No. 51221004)

trolled by motor drivers. With this system, they developed a self-controlled rehabilitation therapy. The proportional-integral-derivative (PID) feedback control has also been widely used in position control. Tjahyono *et al.* (2013) designed a five-fingered hand exoskeleton driven by pneumatic artificial muscles (PAMs) with novel polypyrrole sensors controlled by a PID controller. Azzurra *et al.* (2012) designed a 4-DOF index finger exoskeleton (HANDEXOS) for post-stroke rehabilitation. They modeled the dynamics of an exoskeleton and employed a PID controller for position control. In addition, the force threshold was chosen based on the concern for security. To control the exoskeleton more precisely, some researchers have incorporated friction compensation into the controller. Polotto *et al.* (2012) formulated the model using system identification and modeled the friction dynamics using Stribeck's model, successfully implementing a control system using a PID feedback controller and friction compensation. Schabowsky *et al.* (2010) presented a hand rehabilitation exoskeleton. Compensation algorithms were developed to improve the exoskeleton's back drivability by counteracting gravity, stiction, and kinetic friction.

Thus far, few researchers have implemented force control into their hand exoskeletons. Nakagawara *et al*. (2005) designed a multi-fingered master hand using encounter-type force feedback, which enables unconstrained motion of the operator's finger and natural contact sensation. The torque of joint is calculated according to the system dynamic model for force control. Wege *et al.* (2006) deployed two closed loops in their control method. The inner loop implements position control via a sliding mode control method, and the outer loop handles force control via admittance control. However, they neglected the impedance of the human finger itself. Fang *et al.* (2009) designed an exoskeleton that can distinguish contact and non-contact modes. When the slave hand touches an object, the master exoskeleton finger can generate a force that is equal to the force applied on the slave finger using a force control scheme. In this method, a high-end control hardware system is necessary.

As the exoskeletons appear to be dexterous robot hands, the control methods used in hand exoskeletons could be imitated, especially the methods for impedance control, which controls not only the position and force but also an interaction between the exoskeleton and human body (Hogan, 1985). This method has been applied in an upper-limb exoskeleton (Kiguchi and Hayashi, 2012).

However, the aforementioned control methods consider the human-machine interaction system as a linear time-invariant (LTI) system. As shown in Fig. 1, the exoskeleton robots are nonlinear systems, and the exoskeletons contact human soft tissues associated with a rigid body using an interaction system. Since the performance of this soft tissue cannot be described in a formula, the parameters of the interaction system are uncertain.

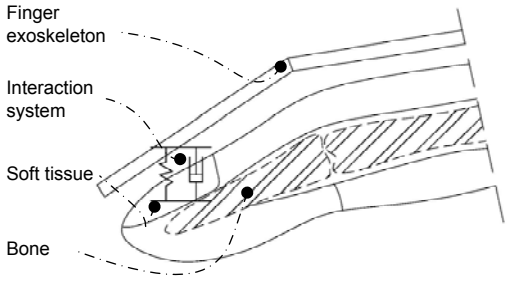

Fig. 1 A human-machine interaction sketch

One of the methods to solve this nonlinear problem is making the controller adaptive to state variables. In addition, the mechanical performance of soft tissue varies in different postures, while we want the system to achieve the desired performance, i.e., a reference model. Obviously, linear controllers cannot be used in this situation. Instead, model reference adaptive control (MRAC) is an effective means, and has been widely used in robot control (Nicosia and Tomei, 1984; Kamnik *et al.*, 1998; Kamal *et al.*, 2010).

As addressed above, impedance control is effective for interaction force control and MRAC is effective for nonlinear systems. So, we combine these two methods and propose a model reference adaptive impedance control (MRAIC) method, applied to an index finger exoskeleton system.

2 Model reference adaptive impedance control method

The MRAIC method is implemented into the hand exoskeleton as shown in Fig. 2. Here, the plant, i.e., the control object, is the dynamics of the human-

machine interaction (HMI) system represented by equation $\dot{\boldsymbol{e}}_{\mathrm{P}} = \boldsymbol{A}_{\mathrm{P}}\boldsymbol{e}_{\mathrm{P}} + \boldsymbol{B}_{\mathrm{P}}\boldsymbol{u}$. It is modeled according to the impedance of a finger. $K_{\mathrm{BC}}(s)$ and $K_{\mathrm{FC}}(s)$ represent an adaptive feedback controller and feedforward controller, respectively. They are derived via the Lyapunov stability theory (Pang and Chui, 2009). Equation $\dot{\boldsymbol{e}}_{\mathrm{m}} = \boldsymbol{A}_{\mathrm{m}}\boldsymbol{e}_{\mathrm{m}} + \boldsymbol{B}_{\mathrm{m}}\boldsymbol{y}_{\mathrm{r}}$ is the reference model for the system. Besides, $\boldsymbol{y}_{\mathrm{r}}$ is the input of the control system, $\boldsymbol{u}$ is the input of the exoskeleton, and $\boldsymbol{e}$ is the error between the reference model and plant.

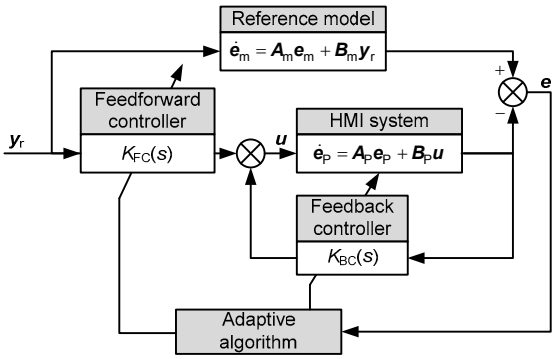

Fig. 2 Control diagram of our proposed model reference adaptive impedance control method

The proposed method is implemented through the following steps:

1. Model the HMI and calculate the state variables;

2. Update the adaptive controllers using the state variables;

3. Calculate the input value of the exoskeleton.

2.1 Plant modeling

As shown in Fig. 3, we assume the interaction system is a mass-spring-damper system. The interaction force varies as the exoskeleton moves to different positions. In other words, the mechanical impedance between the displacement and force varies (Seraji and Colbaugh, 1997). Thus, position control is the inner loop, and impedance control is the outer loop. We will focus on designing the controller for the outer loop. The position control is achieved by motor drivers.

In Fig. 3, X_{H} represents the critical contact position with the finger. When the exoskeleton moves to position X, there is a corresponding force F due to the deformation of soft tissues. In addition, X_{R} corresponds to the desired interaction force F_{R}.

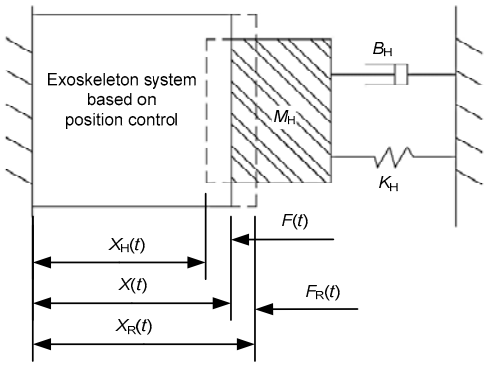

Fig. 3 Exoskeleton and human interaction

The finger mechanical impedance, which in general represents the relationship between motion and force, can be written as follows:

$$G_{\mathrm{H}}(s) = \frac{X_{\mathrm{H}}(s)}{F(s)} = \frac{1}{M_{\mathrm{H}}s^2 + B_{\mathrm{H}}s + K_{\mathrm{H}}}, \qquad (1)$$

where $X_{\mathrm{H}}=X_{\mathrm{E}}-X$ denotes the deformation of the human finger. M_{H}, B_{H}, and K_{H} represent the mass, damping, and stiffness, respectively. Based on the discussion in Section 1, these three parameters are time-variant. Table 1 shows their nominal values and percentages of perturbation relative to the nominal values (Bi *et al.*, 2013).

Table 1 Parameters of the finger impedance

Parameter	Nominal value	Upper band	Lower band
Mass (kg)	0.064	4.7%	−3.6%
Damping (N·s/m)	5.190	1.9%	−1.1%
Stiffness (N/m)	448.3	4.9%	−8.7%

As shown in Fig. 4, the actual impedance is not ideal. Both overshoot and stable final values are perturbative. To improve the performance, we define linear time-invariant (LTI) impedance as the target, which is over-damped. The step responses are compared in Fig. 4.

In a similar manner, the target impedance can be derived as follows:

$$G_{\mathrm{T}}(s) = \frac{X_{\mathrm{T}}(s)}{E_{\mathrm{F}}(s)} = \frac{1}{M_{\mathrm{T}}s^2 + B_{\mathrm{T}}s + K_{\mathrm{T}}}, \qquad (2)$$

where $X_{\mathrm{T}}=X_{\mathrm{R}}-X$ represents the difference between the reference position and actual position, and $E_{\mathrm{F}}=F_{\mathrm{R}}-F$ denotes the difference between the refer-

ence force and actual force. M_T, B_T, and K_T represent the mass, damping, and stiffness, respectively.

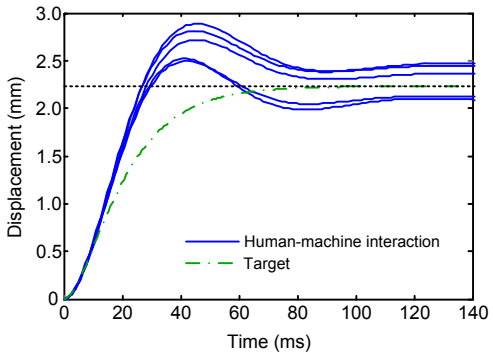

Fig. 4 The step response of human-machine interaction

Using Eqs. (1) and (2), we can obtain

$$E_F(s)=\frac{F_R(s)G_H(s)+X_H(s)-X_R(s)}{G_T(s)+G_H(s)}. \tag{3}$$

According to the final-value theorem, as time goes to infinity, s goes to zero.

$$\begin{aligned}E_{Fss}&=\lim_{s\to 0}E_F(s)=\frac{F_R\dfrac{1}{K_H}+X_H-X_R}{\dfrac{1}{K_T}+\dfrac{1}{K_H}}\\&=\frac{K_TK_H}{K_T+K_H}\left(F_R\frac{1}{K_H}+X_H-X_R\right).\end{aligned} \tag{4}$$

According to Eq. (4), the static error value is affected by the stiffness of the human finger, the stiffness of the target impedance, and the input variables. We can define X_R as follows to eliminate the static error:

$$X_R=F_R\frac{1}{K_H}+X_H. \tag{5}$$

To obtain the error dynamics, we can expand Eq. (3):

$$\begin{aligned}E_F(s)=&\frac{1}{M_Hs^2+B_Hs+K_H+M_Ts^2+B_Ts+K_T}\\&\cdot\big[F_R(s)(M_Ts^2+B_Ts+K_T)\\&+X_H(s)(M_Hs^2+B_Hs+K_H)(M_Ts^2+B_Ts+K_T)\\&-X_R(s)(M_Hs^2+B_Hs+K_H)(M_Ts^2+B_Ts+K_T)\big].\end{aligned} \tag{6}$$

To produce a constant contact force, the reference position X_R is specified to 'penetrate' into the object by a constant amount, i.e., $\dot{X}_R=\ddot{X}_R=0$ and $\dot{X}_H=\ddot{X}_H=0$. Hence, Eq. (6) becomes

$$E_F(s)=\frac{F_R(s)K_T+(X_H(s)-X_R(s))K_HK_T}{(M_H+M_T)s^2+(B_H+B_T)s+(K_H+K_T)}. \tag{7}$$

Change Eq. (7) into the differential form via Laplace inverse transform:

$$\begin{aligned}&\ddot{E}_F(t)+\dot{E}_F(t)\frac{B_T+B_H}{M_T+M_H}+E_F(t)\frac{K_T+K_H}{M_T+M_H}\\&=\frac{F_R(t)K_T+X_H(t)K_TK_H}{M_T+M_H}-\frac{K_TK_H}{M_T+M_H}X_R(t).\end{aligned} \tag{8}$$

As this method is based on the position control inner loop, we transform the input of the error dynamics into an equivalent position:

$$\begin{aligned}&\ddot{E}_F(t)+\dot{E}_F(t)\frac{B_T+B_H}{M_T+M_H}+E_F(t)\frac{K_T+K_H}{M_T+M_H}\\&=\frac{K_TK_H}{M_T+M_H}X_U(t),\end{aligned} \tag{9}$$

where X_U represents the equivalent position:

$$X_U(t)=\frac{F_R(t)}{K_H}+X_H(t)-X_R(t). \tag{10}$$

So we obtain the state space equation:

$$\dot{\boldsymbol{e}}_P=\boldsymbol{A}_P\boldsymbol{e}_P+\boldsymbol{B}_P\boldsymbol{u}, \tag{11}$$

where

$$\boldsymbol{e}_P=[E_F\ \ \dot{E}_F]^T,$$

$$\boldsymbol{A}_P=\begin{bmatrix}0 & 1\\ -\dfrac{K_T+K_H}{M_T+M_H} & -\dfrac{B_T+B_H}{M_T+M_H}\end{bmatrix},$$

$$\boldsymbol{B}_P=\begin{bmatrix}0 & \dfrac{K_TK_H}{M_T+M_H}\end{bmatrix}^T.$$

2.2 Controller design

From Eq. (7), we draw the bode plot for the plant (Fig. 5). Obviously, the error dynamics is stable, but the cutting frequency is approximately 100 Hz, larger than the human movement potential. A too

fast response may have an impact on patients. However, patients cannot bear violent movements caused by the impact, especially in the early stage of rehabilitation. Eq. (8) describes the impedance of HMI, not including the mechanism or the control system's inherent characteristics. Considering the response performance of the system and comfort of the patient, the cutting frequency is preferred to be approximately 10 Hz for the reference model (Fig. 5), such that the exoskeleton can respond to the control system in time and drive the patient's finger gently.

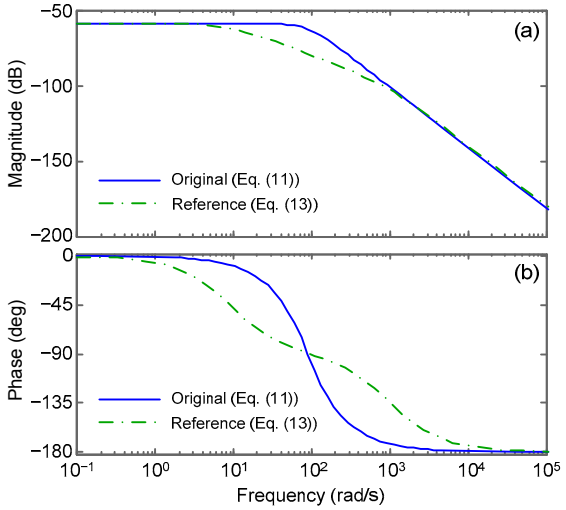

Fig. 5 Open loop system bode plot: (a) magnitude-frequency response; (b) phase-frequency response

Similar to Eq. (10), we transform the input of the error dynamics into an equivalent position:

$$\boldsymbol{y}_{\mathrm{r}}=\boldsymbol{T}\boldsymbol{r}, \tag{12}$$

where

$$\boldsymbol{r}=[F_{\mathrm{R}}\quad X_{\mathrm{H}}\quad X_{\mathrm{R}}]^{\mathrm{T}},\quad \boldsymbol{T}=\begin{bmatrix}\dfrac{1}{K_{\mathrm{H}}} & 1 & -1\end{bmatrix},$$

$$\dot{\boldsymbol{e}}_{\mathrm{m}}=\boldsymbol{A}_{\mathrm{m}}\boldsymbol{e}_{\mathrm{m}}+\boldsymbol{B}_{\mathrm{m}}\boldsymbol{y}_{\mathrm{r}}, \tag{13}$$

and

$$\boldsymbol{e}_{\mathrm{m}}=\begin{bmatrix}E_{\mathrm{m}}\\ \dot{E}_{\mathrm{m}}\end{bmatrix},\ \boldsymbol{A}_{\mathrm{m}}=\begin{bmatrix}0 & 1\\ -\omega^2 & -2\xi\omega\end{bmatrix},\ \boldsymbol{B}_{\mathrm{m}}=\begin{bmatrix}0\\ \dfrac{K_{\mathrm{T}}K_{\mathrm{H}}}{M_{\mathrm{T}}+M_{\mathrm{H}}}\end{bmatrix}.$$

Herein ω represents the cut-off frequency of the reference model and ξ represents the damping coefficient.

The input control command is defined as follows:

$$\boldsymbol{u}=\boldsymbol{K}_{\mathrm{FC}}\boldsymbol{y}_{\mathrm{r}}+\boldsymbol{K}_{\mathrm{BC}}\boldsymbol{e}_{\mathrm{P}}, \tag{14}$$

where $\boldsymbol{K}_{\mathrm{FC}}$ and $\boldsymbol{K}_{\mathrm{BC}}$ are the feedforward controller and feedback controller, respectively. Both of them are adapted to the state variables of the system.

Substituting Eq. (14) into Eq. (11), we obtain

$$\dot{\boldsymbol{e}}_{\mathrm{P}}=(\boldsymbol{A}_{\mathrm{P}}+\boldsymbol{B}_{\mathrm{P}}\boldsymbol{K}_{\mathrm{BC}})\boldsymbol{e}_{\mathrm{P}}+\boldsymbol{B}_{\mathrm{P}}\boldsymbol{K}_{\mathrm{FC}}\boldsymbol{y}_{\mathrm{r}}. \tag{15}$$

Thus, we have the state error equation of the system:

$$\dot{\boldsymbol{e}}=\boldsymbol{A}_{\mathrm{m}}\boldsymbol{e}+(\boldsymbol{A}_{\mathrm{m}}-\boldsymbol{A}_{\mathrm{P}}-\boldsymbol{B}_{\mathrm{P}}\boldsymbol{K}_{\mathrm{BC}})\boldsymbol{e}_{\mathrm{P}}+(\boldsymbol{B}_{\mathrm{m}}-\boldsymbol{B}_{\mathrm{P}}\boldsymbol{K}_{\mathrm{FC}})\boldsymbol{y}_{\mathrm{r}}. \tag{16}$$

Assume that the adjustable system matches the reference model when $\boldsymbol{K}_{\mathrm{BC}}(t)=\boldsymbol{K}_{\mathrm{B0}}$ and $\boldsymbol{K}_{\mathrm{FC}}(t)=\boldsymbol{K}_{\mathrm{F0}}$. As a result, we obtain

$$\boldsymbol{A}_{\mathrm{P}}+\boldsymbol{B}_{\mathrm{P}}\boldsymbol{K}_{\mathrm{B0}}=\boldsymbol{A}_{\mathrm{m}},\ \ \boldsymbol{B}_{\mathrm{P}}\boldsymbol{K}_{\mathrm{F0}}=\boldsymbol{B}_{\mathrm{m}}. \tag{17}$$

Substituting Eq. (17) into Eq. (16) to eliminate $\boldsymbol{A}_{\mathrm{P}}$ and $\boldsymbol{B}_{\mathrm{P}}$ yields

$$\dot{\boldsymbol{e}}=\boldsymbol{A}_{\mathrm{m}}\boldsymbol{e}+\boldsymbol{B}_{\mathrm{m}}\boldsymbol{K}_{\mathrm{F0}}^{-1}\tilde{\boldsymbol{K}}_{\mathrm{B}}\boldsymbol{e}_{\mathrm{P}}+\boldsymbol{B}_{\mathrm{m}}\boldsymbol{K}_{\mathrm{F0}}^{-1}\tilde{\boldsymbol{K}}_{\mathrm{F}}\boldsymbol{y}_{\mathrm{r}}, \tag{18}$$

where

$$\tilde{\boldsymbol{K}}_{\mathrm{B}}=\boldsymbol{K}_{\mathrm{B0}}-\boldsymbol{K}_{\mathrm{BC}},\ \ \tilde{\boldsymbol{K}}_{\mathrm{F}}=\boldsymbol{K}_{\mathrm{F0}}-\boldsymbol{K}_{\mathrm{FC}}.$$

The Lyapunov stability theory is used to design the controller. We define the Lyapunov function as

$$V=\boldsymbol{e}^{\mathrm{T}}\boldsymbol{P}\boldsymbol{e}+\mathrm{tr}(\tilde{\boldsymbol{K}}_{\mathrm{B}}^{\mathrm{T}}\boldsymbol{P}_{\mathrm{B}}^{-1}\tilde{\boldsymbol{K}}_{\mathrm{B}})+\mathrm{tr}(\tilde{\boldsymbol{K}}_{\mathrm{F}}^{\mathrm{T}}\boldsymbol{P}_{\mathrm{F}}^{-1}\tilde{\boldsymbol{K}}_{\mathrm{F}}), \tag{19}$$

where $\boldsymbol{P}$, $\boldsymbol{P}_{\mathrm{B}}$, and $\boldsymbol{P}_{\mathrm{F}}$ are symmetric positive matrixes. Taking the derivative of the Lyapunov function with respect to time yields

$$\begin{aligned}\dot{V}=&\boldsymbol{e}^{\mathrm{T}}(\boldsymbol{A}_{\mathrm{m}}^{\mathrm{T}}\boldsymbol{P}+\boldsymbol{P}\boldsymbol{A}_{\mathrm{m}})\boldsymbol{e}\\&+2\mathrm{tr}(\dot{\tilde{\boldsymbol{K}}}_{\mathrm{B}}^{\mathrm{T}}\boldsymbol{P}_{\mathrm{B}}^{-1}\tilde{\boldsymbol{K}}_{\mathrm{B}}+\boldsymbol{e}_{\mathrm{P}}\boldsymbol{e}^{\mathrm{T}}\boldsymbol{P}\boldsymbol{B}_{\mathrm{m}}\boldsymbol{K}_{\mathrm{F0}}^{-1}\tilde{\boldsymbol{K}}_{\mathrm{B}})\\&+2\mathrm{tr}(\dot{\tilde{\boldsymbol{K}}}_{\mathrm{F}}^{\mathrm{T}}\boldsymbol{P}_{\mathrm{F}}^{-1}\tilde{\boldsymbol{K}}_{\mathrm{F}}+\boldsymbol{y}_{\mathrm{r}}\boldsymbol{e}^{\mathrm{T}}\boldsymbol{P}\boldsymbol{B}_{\mathrm{m}}\boldsymbol{K}_{\mathrm{F0}}^{-1}\tilde{\boldsymbol{K}}_{\mathrm{F}}).\end{aligned} \tag{20}$$

According to the Lyapunov theorem of stability, we obtain

$$\boldsymbol{A}_{\mathrm{m}}^{\mathrm{T}}\boldsymbol{P}+\boldsymbol{P}\boldsymbol{A}_{\mathrm{m}}=-\boldsymbol{Q},\quad \boldsymbol{Q}=\boldsymbol{Q}^{\mathrm{T}}>\boldsymbol{0}. \tag{21}$$

To ensure a negative definite $\dot{V}$, we obtain

$$\begin{cases} \dot{\boldsymbol{K}}_{\mathrm{B}} = -\boldsymbol{P}_{\mathrm{B}} \boldsymbol{K}_{\mathrm{F0}}^{-\mathrm{T}} \boldsymbol{B}_{\mathrm{m}}^{\mathrm{T}} \boldsymbol{P} \boldsymbol{e} \boldsymbol{e}_{\mathrm{P}}^{\mathrm{T}}, \\ \dot{\boldsymbol{K}}_{\mathrm{F}} = -\boldsymbol{P}_{\mathrm{F}} \boldsymbol{K}_{\mathrm{F0}}^{-\mathrm{T}} \boldsymbol{B}_{\mathrm{m}}^{\mathrm{T}} \boldsymbol{P} \boldsymbol{e} \boldsymbol{y}_{\mathrm{r}}^{\mathrm{T}}. \end{cases} \tag{22}$$

Since $\boldsymbol{P}_{\mathrm{B}}$, $\boldsymbol{P}_{\mathrm{F}}$, and $\boldsymbol{K}_{\mathrm{F0}}$ are artificially constructed, Eq. (22) could be rewritten following the adaptive control law:

$$\begin{cases} \dot{\boldsymbol{K}}_{\mathrm{B}} = \boldsymbol{R}_1 \boldsymbol{B}_{\mathrm{m}}^{\mathrm{T}} \boldsymbol{P} \boldsymbol{e} \boldsymbol{e}_{\mathrm{P}}^{\mathrm{T}}, \\ \dot{\boldsymbol{K}}_{\mathrm{F}} = \boldsymbol{R}_2 \boldsymbol{B}_{\mathrm{m}}^{\mathrm{T}} \boldsymbol{P} \boldsymbol{e} \boldsymbol{y}_{\mathrm{r}}^{\mathrm{T}}, \end{cases} \tag{23}$$

where $\boldsymbol{R}_1$ and $\boldsymbol{R}_2$ are the coefficients of the feedback controller and feedforward controller, respectively.

3 Simulations and experiments

This section illustrates the performance of our designed controllers via numerical simulations in MATLAB and experiments using our index finger exoskeleton. As shown in Fig. 6, the simulation involves the extension posture. The exoskeleton could move to the desired position precisely via the inner loop of the control system. When the exoskeleton makes a small displacement, the soft tissue at the dorsal side of the finger shows mechanical impedance. The force between the exoskeleton and the finger can be measured by a force sensor.

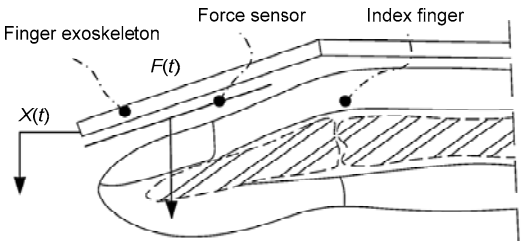

Fig. 6 Simulation diagram

The parameters of finger impedance, including nominal values of the second order system and their perturbation range, are estimated via system identification. For the simulations here, we use the parameters under extension posture (Table 2).

The experiments are also set under extension posture (Fig. 7). The exoskeleton has two active DOFs at the metacarpophalangeal (MP) joint and proximal interphalangeal (PIP) joint, respectively, and one coupling DOF at the distal interphalangeal (DIP) joint. Two Maxon DC motors rotate screws, driving the multi-linkages to make the joints of the exoskeleton rotate. The lower computer (DSP) sends commands to motor drivers via the controller area network (CAN) bus, and collects haptic data using acquisition circuits.

Table 2 Human-machine interaction impedance

Impedance	Mass (kg)	Damping (N·s/m)	Stiffness (N/m)
Actual	0.064	5.19	448.3
Target	0.050	10.00	448.3

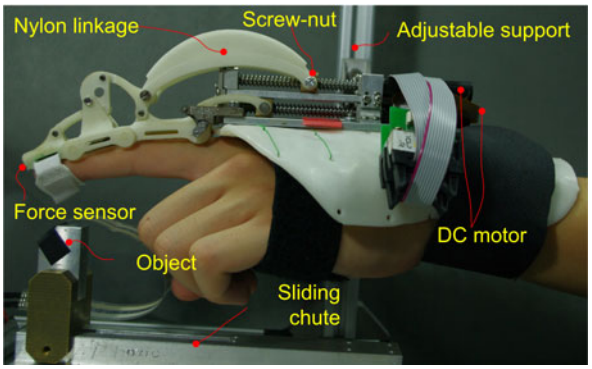

Fig. 7 Index exoskeleton system

3.1 Time domain simulations and experiments

Simulations and experiments in the time domain intuitively illustrate the performance of the MRAIC method. To make the results more convincible, a PID controller is implemented for comparison. We perform two groups of tests, square wave tracking and sinusoidal tracking.

Square wave tracking makes the system switch between dynamic and static. Fig. 8 shows the reference input, simulation using MRAIC in Matlab, an experiment using MRAIC, and an experiment using PID. Both the simulation and experiment of MRAIC can get stabilized, while the PID method cannot. As mentioned above, the interaction system is time-variant and nonlinear, and thus a PID controller is not suitable. The indexes are listed in Table 3. The MRAIC method outperforms PID in terms of stabilization and speed. The MRAIC simulation and experiment are similar except for the maximum overshoot. Since the command cannot be executed immediately, the exoskeleton moves on for a small dis-

placement, which leads to a higher overshoot. In other words, time delay in the control system results in this difference.

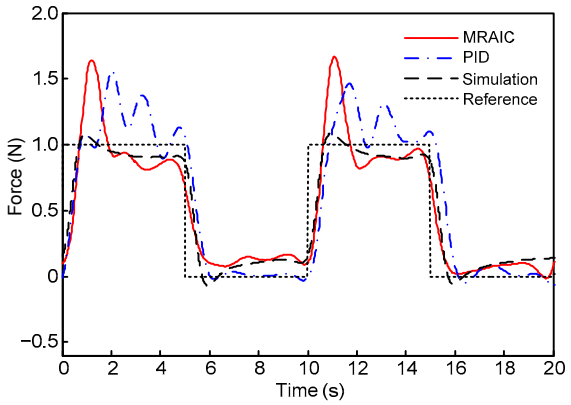

Fig. 8 Comparison of square wave tracking

Table 3 Indexes in square wave tracking

No.	Method	E_S (N)	T_P (s)	T_S (s)	A_M (%)
1	Simulation	0.09	0.94	2.05	8
	MRAIC	0.16	1.21	2.85	64
	PID	–	2.06	–	56
2	Simulation	0.10	0.95	2.24	8
	MRAIC	0.11	1.10	2.74	66
	PID	–	1.72	–	46

E_S: steady error; T_P: peak time; T_S: setting time; A_M: maximum overshoot

Sinusoidal tracking is aimed to verify the continuous dynamic performance. In Fig. 9, both the MRAIC simulation and experiment can follow the reference signal better than the PID experiment in terms of the maximum error and root mean square error (Table 4). Additionally, the phase errors of MRAIC are smaller than those of PID.

Comparison of the MRAIC and PID controllers in the two groups of tests shows that MRAIC has stronger robustness even when the system suffers from saltus and the parameters are perturbative.

3.2 Frequency domain simulations

To further analyze the performance of the system, we conduct some frequency response simulations. In each simulation we change only one parameter to observe the influence on the system.

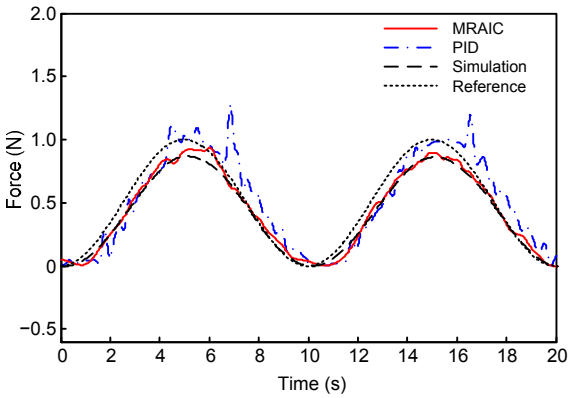

Fig. 9 Comparison of sinusoidal tracking

Table 4 Indexes in sinusoidal wave tracking

Method	E_M (N)	E_P (°)	RMS
Simulation	0.16	4.05	0.0885
MRAIC	0.18	5.69	0.0871
PID	0.29	11.16	0.1288

E_M: maximum error; E_P: phase error; RMS: root mean square error

The perturbation range is set larger than the range measured to evaluate the performance of the system as much as possible. Each value increases from 10% nominal to 200% nominal. Figs. 10–12 show the frequency responses. The shadows mark out the variation ranges, all of which are concentrated in the low frequency stages. As shown in Section 2.2, a fast frequency response may have an impact on patients. The cutting frequency of the reference model is set at 10 Hz. Thus, in all frequency simulations, the frequency response above 10 Hz decays greatly. The change caused by finger mass is below 5 Hz, and its gain increases with increasing mass. The difference of peak gain (PG) is approximately 25 dB. Although the variations of both damping and stiffness do not change the PG, they influence the different frequency bounds. The former is less than 0.06 Hz and the latter less than 1 Hz. The human-machine system usually works in a limited low frequency bound (from 10^{-1} to 10^{1}); therefore, mass and stiffness influence the system significantly.

After analyzing the influence of human finger impedance, we explore how the parameters in the controller influence the system. In the adaptive controller, the symmetric positive matrixes $\boldsymbol{R}_1$, $\boldsymbol{R}_2$, and $\boldsymbol{P}$ are set manually. We define them as unit matrixes

multiplied by a coefficient. Figs. 13–15 correspond to the three matrixes. Similar to the simulations above, the changes are concentrated in the low frequency bound. For the variation of $\boldsymbol{R}_1$, it is between 0.02 Hz and 3 Hz. For the variation of $\boldsymbol{R}_2$, it is below 0.015 Hz. The upper bound of the variation of $\boldsymbol{P}$ is 5 Hz. In addition, the differences of peak gain are approximately 32 dB and 52 dB for $\boldsymbol{R}_1$ and $\boldsymbol{P}$, respectively.

The shadow areas show the perturbations caused by different variables. According to the influencing range of each factor, we can determine which factor to use in a specific bound. The shadow areas are similar for these two groups of frequency response.

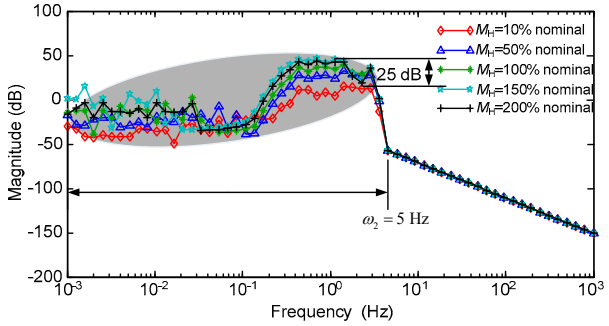

Fig. 10 Influence of finger mass

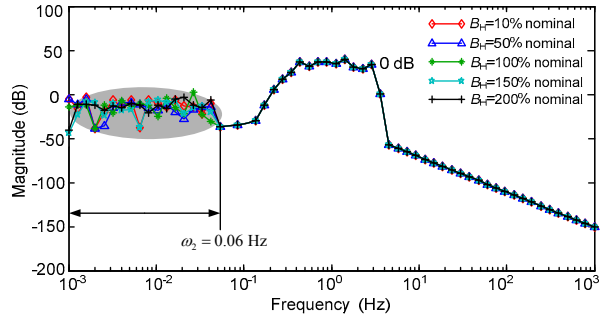

Fig. 11 Influence of finger damping

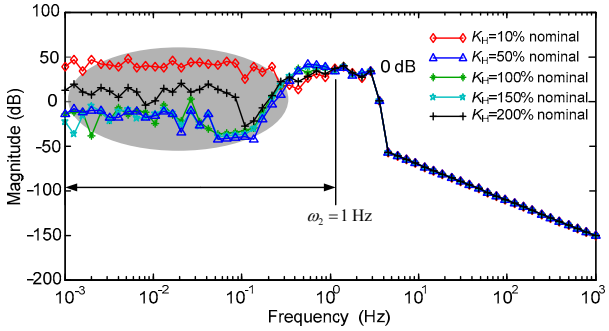

Fig. 12 Influence of finger stiffness

The shadow in Fig. 11 is smaller than that in Fig. 14. The shadow in Fig. 15 almost contains those in both Figs. 10 and 12. Thus, we could attempt to make the $\boldsymbol{R}_2$ in the feedforward controller adaptive to the perturbed damping in finger impedance and make the $\boldsymbol{P}$ in both controllers adaptive to deal with the uncertainties of mass and stiffness in finger impedance.

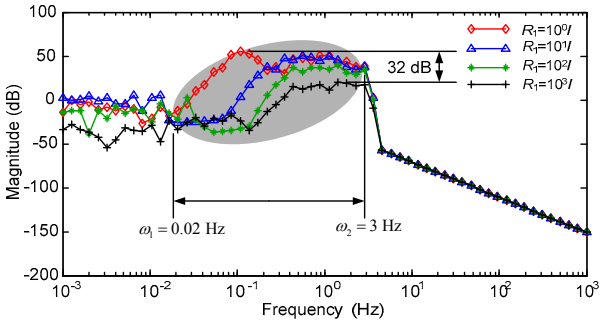

Fig. 13 Influence of R_1 in the feedback controller

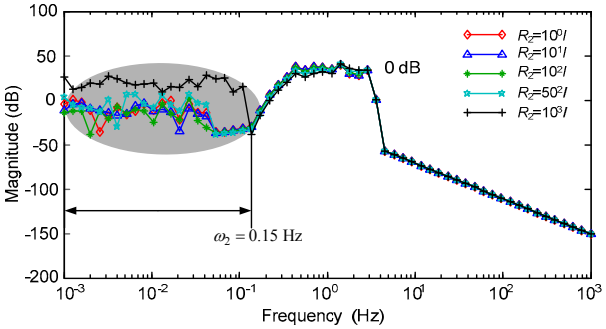

Fig. 14 Influence of R_2 in the feedforward controller

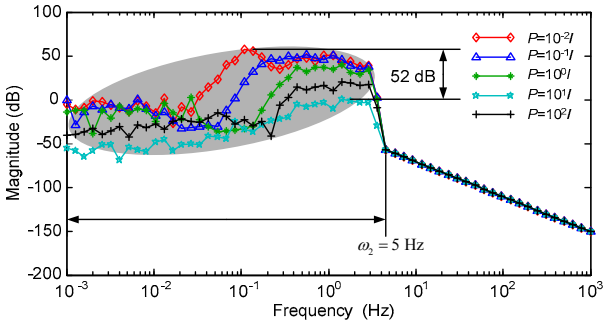

Fig. 15 Influence of P

4 Conclusions

We present a model reference adaptive impedance control (MRAIC) method for an index finger exoskeleton, including modeling HMI dynamics,

reference model designs, and controller designs supported by the Lyapunov theory.

Based on the comparison in simulations and experiments using the MRAIC method, the modeling is basically consistent with the real situation, when ignoring the time delay in the control system. Besides, the comparison of experiments using MRAIC and PID indicates that the MRAIC scheme performs better in terms of stabilization and speed. In other words, MRAIC is effective for the nonlinear HMI problem in hand exoskeleton control, where PID or other linear methods could not work well. The frequency simulation reflects the influence of different parameters on the control system. The system performance is optimal in the bound between 0.1 and 5 Hz, which is the frequency range of human body movement.

Future work will involve improvements in two aspects: solving the time delay of the system, which is an unstable factor; optimizing the parameters $\boldsymbol{R}_1$, $\boldsymbol{R}_2$, and $\boldsymbol{P}$ according to the state variables instead of tuning empirically.

References

Azzurra, C., Nicola, V., Francesco, G., *et al*., 2012. Mechatronic design and characterization of the index finger module of a hand exoskeleton for post-stroke rehabilitation. *IEEE/ASME Trans. Mechatron.*, **17**(5):884-894. [doi:10.1109/TMECH.2011.2144614]

Bi, Q., Yang, C.J., Deng, X.L., *et al*., 2013. Contacting mechanical impedance of human finger based on uncertain system. IEEE/ASME Int. Conf. on Advanced Intelligent Mechatronics, p.1619-1624. [doi:10.1109/AIM.2013.6584328]

Fang, H.G., Xie, Z.W., Liu, H., *et al*., 2009. An exoskeleton force feedback master finger distinguishing contact and non-contact mode. IEEE/ASME Int. Conf. on Advanced Intelligent Mechatronics, p.1059-1064. [doi:10.1109/AIM.2009.5229726]

Hogan, N., 1985. Impedance control: an approach to manipulation: part I—theory. *J. Dynam. Syst. Meas. Contr.*, **107**(1):1-7.

Huo, W.G., Huang, J., Wang, Y.J., *et al*., 2011. Control of upper-limb power-assist exoskeleton based on motion intention recognition. Int. Conf. on Robotics and Automation, p.2243-2248. [doi:10.1109/ICRA.2011.5980483]

Kamal, H.S., Hamid, M., Farrokh, J.S., 2010. Model reference adaptive control design for a teleoperation system with output prediction. *J. Intell. Robot. Syst.*, **59**:319-339. [doi:10.1007/s10846-010-9400-4]

Kamnik, R., Matko, D., Bajd, T., 1998. Application of model reference adaptive control to industrial robot impedance control. *J. Intell. Robot. Syst.*, **22**:153-163. [doi:10.1023/A:1007932701318]

Kiguchi, K., Hayashi, Y., 2012. An EMG-based control for an upper-limb power-assist exoskeleton robot. *IEEE Trans. Syst. Man. Cybern. B*, **42**:1064-1071. [doi:10.1109/TSMCB.2012.2185843]

Nakagawara, S., Kajimoto, H., Kawakami, N., *et al*., 2005. An encounter-type multi-fingered master hand using circuitous joints. Proc. IEEE Int. Conf. on Robotics and Automation, p.2667-2672. [doi:10.1109/ROBOT.2005.1570516]

Nicosia, S., Tomei, P., 1984. Model reference adaptive control algorithms for industrial robots. *Automatica*, **20**(5):635-644. [doi:10.1016/0005-1098(84)90013-X]

Pang, Z.H., Chui, H., 2009. System Identification and Adaptive Control. Beijing University of Aeronautics and Astronautics Press, Beijing, p.78-80 (in Chinese).

Polotto, A., Modulo, F., Flumian, F., *et al.*, 2012. Index finger rehabilitation/assistive device. 4th IEEE RAS/EMBS Int. Conf. on Biomedical Robotics and Biomechatronics, p.1518-1523. [doi:10.1109/BioRob.2012.6290676]

Prange, G.B., Jannink M.J.A., Groothuis-Oudshoorn, C.G.M., *et al.*, 2006. Systematic review of the effect of robot-aided therapy on recovery of the hemiparetic arm after stroke. *J. Rehabil. Res. Devel.*, **43**(2):171-183. [doi:10.1682/JRRD.2005.04.0076]

Schabowsky, C.N., Godfrey, S.B., Holley, R.J., *et al.*, 2010. Development and pilot testing of HEXORR: Hand EXOskeleton Rehabilitation Robot. *J. NeuroEng. Rehabil.*, **7**:36. [doi:10.1186/1743-0003-7-36]

Seraji, H., Colbaugh, R., 1997. Force tracking in impedance control. *Int. J. Robot. Res.*, **16**(1):97-117. [doi:10.1177/027836499701600107]

Takahashi, C.D., Der-Yeghiaian, L., Le, V., *et al.*, 2008. Robot-based handmotor therapy after stroke. *Brain*, **131**(2):425-437. [doi:10.1093/brain/awm311]

Tjahyono, A.P., Aw, K.C., Devaraj, H., *et al*., 2013. A five-fingered hand exoskeleton driven by pneumatic artificial muscles with novel polypyrrole sensors. *Ind. Robot Int. J.*, **40**(3):251-260. [doi:10.1108/01439911311309951]

Ueki, S., Kawasakia, H., Itoa, S., *et al*., 2012. Development of a hand-assist robot with multi-degrees-of-freedom for rehabilitation therapy. *IEEE/ASME Trans. Mechatron.*, **17**(1):136-146. [doi:10.1109/TMECH.2010.2090353]

Wege, A., Kondak, K., Hommel, G., 2006. Force control strategy or a hand exoskeleton based on sliding mode position control. Proc. IEEE/RSJ Int. Conf. on Intelligent Robots and Systems, p.4615-4620. [doi:10.1109/IROS.2006.282169]